

Comparative study of in situ N₂ rotational Raman spectroscopy methods for probing energy thermalisation processes during spin-exchange optical pumping

Hayley Newton · Laura L. Walkup · Nicholas Whiting · Linda West · James Carriere · Frank Havermeyer · Lawrence Ho · Peter Morris · Boyd M. Goodson · Michael J. Barlow

Received: 13 June 2013 / Accepted: 12 July 2013
© Springer-Verlag Berlin Heidelberg 2013

Abstract Spin-exchange optical pumping (SEOP) has been widely used to produce enhancements in nuclear spin polarisation for hyperpolarised noble gases. However, some key fundamental physical processes underlying SEOP remain poorly understood, particularly in regards to how pump laser energy absorbed during SEOP is thermalised, distributed and dissipated. This study uses in situ ultra-low frequency Raman spectroscopy to probe rotational temperatures of nitrogen buffer gas during optical pumping under conditions of high resonant laser flux and binary Xe/N₂ gas mixtures. We compare two methods of collecting the Raman scattering signal from the SEOP cell: a conventional orthogonal arrangement combining intrinsic spatial filtering with the utilisation of the internal baffles of the Raman spectrometer, eliminating probe laser light and Rayleigh scattering, versus a new in-line modular design that uses ultra-narrowband notch filters to remove such unwanted contributions. We report a ~23-fold improvement in detection sensitivity using the in-line module, which leads to faster data acquisition and more accurate

real-time monitoring of energy transport processes during optical pumping. The utility of this approach is demonstrated via measurements of the local internal gas temperature (which can greatly exceed the externally measured temperature) as a function of incident laser power and position within the cell.

1 Introduction

Conventional nuclear magnetic resonance (NMR) spectroscopy and imaging (MRI) suffer from inherently low detection sensitivity; even in the highest available magnetic fields, the equilibrium nuclear spin polarisation is very low ($\sim 10^{-4}$ – 10^{-6}). In an effort to combat this sensitivity issue, the increased nuclear spin polarisation of hyperpolarised (HP) noble gases (e.g. ³He, ¹²⁹Xe, and ⁸³Kr) has attracted attention for many diverse MR applications [1], including biomedical MRI of human lung space [2–4], probing porous materials and surfaces [5], and studying host–guest interactions of molecules [6–9]. ³He has a higher gyromagnetic ratio, but ¹²⁹Xe is attractive due to its far wider chemical shift range making it a sensitive MR probe [1], as well as greater physiological solubility and lipophilicity [1]. Additionally, ¹²⁹Xe is naturally abundant, and due to the worldwide ³He shortage [10], there exists an emerging market for HP ¹²⁹Xe technology.

HP ¹²⁹Xe is produced via spin-exchange optical pumping (SEOP) [11], a two-step process by which the angular momentum from circularly polarised laser light is absorbed by the electronic spins of an alkali metal vapour (e.g. Rb or Cs [12]), and then transferred to the nuclear spins of ¹²⁹Xe via collisions. Our previous work studying HP ¹²⁹Xe production at elevated Xe densities and high resonant laser flux [12–14] has led to improvements in Xe polarisation

H. Newton · N. Whiting · P. Morris · M. J. Barlow (✉)
Sir Peter Mansfield Magnetic Resonance Centre,
University of Nottingham, Nottingham NG7 2RD, UK
e-mail: michael.barlow@nottingham.ac.uk

L. L. Walkup · B. M. Goodson
Department of Chemistry and Biochemistry,
Southern Illinois University, Carbondale, IL 62901, USA

Present Address:
N. Whiting
The University of Texas MD Anderson Cancer Center,
1515 Holcombe Blvd, Houston, TX 77030, USA

L. West · J. Carriere · F. Havermeyer · L. Ho
Ondax, Inc., 850 E. Duarte Road, Monrovia, CA 91016, USA

(P_{Xe}), culminating in the recent design of ‘open-source’ clinical xenon polarisers capable of producing HP ^{129}Xe with P_{Xe} values approaching unity, despite the use of Xe-rich gas mixtures [15, 16].

Despite decades of study, some aspects of SEOP remain poorly understood, particularly under the demanding conditions of high resonant laser flux and Xe densities. One such facet concerns the transport of energy within the SEOP chamber (or ‘OP cell’). Nitrogen is often added as a buffer gas to quench fluorescent re-emission (and other undesirable energetic processes [17]) from electronically excited alkali metal atoms via radiationless, two-body (Rb/N_2) collisions. However, these processes result in the accumulation of large amounts of energy in the ro-vibrational manifold of the N_2 buffer gas. In turn, this energy may be thermally distributed to other species throughout the cell in a heterogeneous fashion (with implications for various aspects of the SEOP process), and eventually dissipated to the cell walls and surroundings. Previous work by Walter et al. [18] explored the rotational and vibrational temperatures of N_2 in OP cells via Raman spectroscopy, performed with an orthogonal arrangement for excitation and collection, and subsequent fitting of the recorded Raman intensities to a Boltzmann model. N_2 rotational temperatures of up to ~ 200 °C above the apparent temperature for the exterior surface of the OP cell were reported for SEOP under relatively modest conditions, e.g. ≤ 15 W of ~ 2 nm full-width half maximum (FWHM) laser light with a $^4\text{He}/\text{N}_2$ gas mixture [18]. Walter et al. concluded that probing the outer surface temperature of the OP cell was often a poor indicator of the actual internal gas temperature compared to Raman measurements, given that the N_2 rotational temperature, T_{N_2} , should quickly equilibrate with the translational temperature of N_2 and the other gas species in the cell. We have recently extended such work to the study of Rb/Xe SEOP with high resonant laser flux and high Xe densities [19, 20], and observed much larger temperature differences between the external and internal measurements. Other studies to examine energy transport in optical pumping include work performed by Parnell et al. [21] using diffusion sensitised gradients to measure laser heating, as well as numerical simulations of the production of HP ^{129}Xe by Fink et al. [22]. To further the study of energy transport during SEOP, here we introduce a new method for recording the Stokes/anti-Stokes rotational Raman lines used to determine the local internal gas temperature during optical pumping. We compare this method, a fibre-coupled ‘in-line’ module with ultra-narrow-band notch filters, with our previous home-built orthogonal arrangement [19, 20] for collecting Raman data during SEOP. The utility of the ~ 23 -fold sensitivity improvement provided by the in-line module is demonstrated with measurements of the internal gas temperature

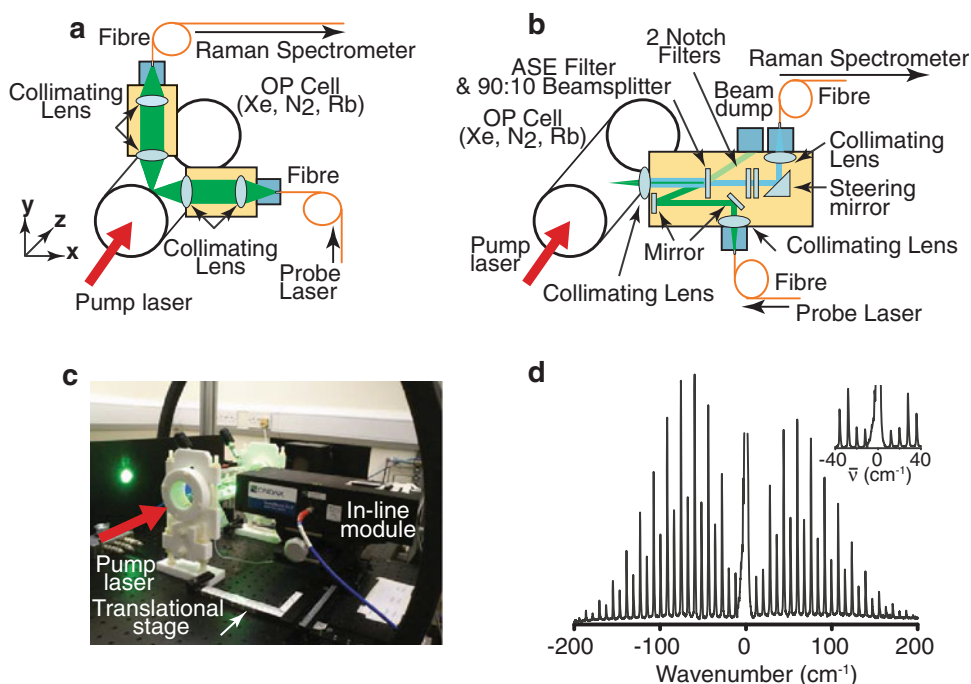
elevation as a function of position and incident laser power, including a comparison of the effects of using frequency-narrowed compared to broadband lasers for SEOP.

2 Methods

In order to record a sufficiently complete rotational Raman spectrum, it is necessary to suppress the scattered ‘probe’ laser signal well enough to resolve the much weaker Raman lines that may be only a few tens of wavenumbers away. Therefore, to observe such ultra-low frequency rotational Raman spectra, we have employed two contrasting assemblies. The first (Fig. 1a) has already been discussed in Refs. [19, 20] and has demonstrated our initial results using Raman spectroscopy to probe T_{N_2} during SEOP. Briefly, the probe laser source (Coherent ‘Verdi’, 5 W, 532 nm) is fibre-coupled to a modular optical lens assembly near the OP cell, collimated, and then focused to a sub-millimetre point within the OP cell (along the x -axis) using a planoconvex lens; the Raman scattering is collected at a 90° angle to the laser source (i.e. along the y -axis), focused onto a 50- μm fibre, and fibre-coupled to the Raman spectrometer. Laser and Rayleigh scattering are spatially filtered using the internal baffles of the Raman spectrometer. Our new approach uses an in-line (confocal) module (Fig. 1b, c) for excitation and detection of the Raman transitions along the same optical path (i.e. x -axis), custom-designed for our application in collaboration with Ondax Incorporated (XLF-C). The same 532 nm laser was used as the probe for the Raman system and was subsequently fibre-coupled into a double 1-m Horiba Jobin–Yvon U1000 Raman Spectrometer with an Andor Newton thermoelectrically cooled electron-multiplying CCD. The in-line module contains two SureBlockTM ultra-narrow-band notch filters, which allow both Stokes and anti-Stokes lines to be viewed simultaneously and increase the system’s capacity to resolve ultra-low frequency Raman lines, as well as one NoiseBlockTM ultra-narrow-band beamsplitter filter that improves the spectrum of the incoming probe beam by reducing any laser sidebands, spontaneous laser diode emissions, or fibre-induced fluorescence. The NoiseBlock filter also acts as a spectrally sensitive 90:10 beamsplitter that transmits collected Raman signals and reduces Rayleigh scattered light by an order of magnitude. This system is capable of being easily translated to allow three-dimensional temperature mapping of the OP cell.

The OP cell under investigation is a 2.5 cm diameter, 15 cm long Pyrex glass cylinder coated with SurfaSilTM siliconising agent and filled with Rb (~ 500 mg), Xe (100 torr), and N_2 (1,900 torr), Fig. 1. The OP cell is heated by a 400-W heat pipe and controlled by a CAL9500 temperature controller, with corresponding Pt100 sensors

Fig. 1 Schematic of (a) orthogonal set-up (previously reported in Refs. [19, 20]) and (b) in-line module for excitation and detection for in situ Raman spectroscopy. c Corresponding photograph of the in-line module. The in-line module is mounted onto a translational stage to allow three-dimensional mapping of T_{N_2} within the cell. d Typical background-corrected rotational Raman spectrum from N_2 gas within OP cell showing the full ranges of Stokes and anti-Stokes scattering frequencies centred around (and plotted as a difference in frequency from) the 532 nm (Rayleigh scattered) probe laser line. The inset shows a close-up of the ultra-low frequency region that is spectrally resolvable using the in-line apparatus



on the oven inlet and outlet. Raman temperature data were acquired in three-second acquisitions to ensure nearly ‘real-time’ information. For demonstration, experiments involving the in-line module and two ‘pump’ (SEOP) lasers with similar overall laser output powers were compared: broadband (QPC Brightlase Ultra-100; ~ 2.13 nm FWHM) and frequency-narrowed (QPC Brightlock Ultra-100; ~ 0.26 nm FWHM).

Raman data were analysed by first applying a baseline correction to the spectra, then fitting each peak to a Gaussian line shape and obtaining peak heights, $S(J)$, for six of the Stokes lines ($J = 4, 6, 8, 10, 12$). These values were then linearly fit using $J(J + 1)$ versus $\ln [S(J) 2(2J + 3)] / (3(J + 1)(J + 2))$, according to the equations discussed by Hickman et al. [23]. This process results in a line with a slope equal to Bhc/kT , from which the rotational temperature, T , of the system can be computed using the rotational constant for N_2 ($B \approx 2 \text{ cm}^{-1}$), Planck’s constant (h), the speed of light (c), and Boltzmann’s constant (k). The error bars of the calculated temperature data points reflect the fit error of these plots.

3 Results and discussion

When utilising the orthogonal arrangement [19, 20] (Fig. 1a), contributions from Rayleigh scattering and the probe laser are minimised by exciting and detecting along different axes (x and y , respectively), as well as spatially filtered by the internal baffles of the Raman spectrometer. However, sub-mm³ accuracy is needed for aligning the

focal points of the excitation and receive optics; this critical alignment is tedious to set up and prone to drift over time. In contrast, the in-line module uses two ultra-narrow-band notch filters, with an optical density greater than 4 and FWHM of 0.35 nm for each filter, to allow transmission of the Raman light while dramatically reducing the infiltration of laser light and Rayleigh scattering into the Raman spectrometer. The application of these filters enables ultra-low frequency Stokes and anti-Stokes Raman scattering [24] peaks to be resolved as close as 10 cm^{-1} from the probe laser line (Fig. 1d).

Examples of typical rotational Raman spectra acquired with the conventional ‘orthogonal’ and ‘in-line’ set-ups are shown in Fig. 2a, b, respectively. The spectra, obtained under identical conditions from a cell containing 100 torr Xe/1,900 torr N_2 , were each acquired over 15 s at room temperature (in the absence of pump laser irradiation). The in-line module was found to provide ~ 23 -fold improved SNR, which translates directly into more precise temperature measurements, as indicated by the corresponding temperature calibration plots (Fig. 2c, d). One complication of the in-line module is the contribution of signals arising from Raman scattering from atmospheric N_2 and O_2 along the optics path outside of the SEOP cell, as manifested by the appearance of the small O_2 peaks in Fig. 2b (note that the molar scattering intensity of O_2 is roughly twice that of N_2 [25]). Removal of these unwanted contributions was attempted by collecting background spectra using an evacuated OP cell. However, slight spectral drifts caused the subtraction of these peaks to lead to non-realistic difference spectra resulting in poorer fits to the

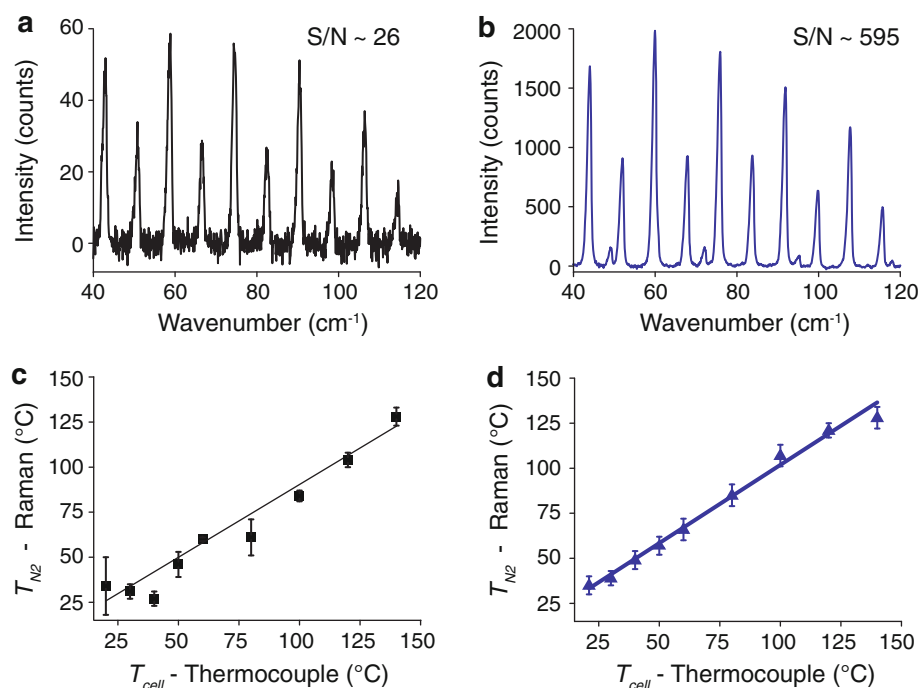


Fig. 2 Comparison of typical rotational Raman spectra from N_2 gas at 24 °C using either the ‘orthogonal’ detection system (**a**) or the ‘in-line’ module (**b**). Spectra were obtained under identical conditions (OP cell containing 100 torr Xe/1,900 torr N_2 , 15 s acquisition time, no pump laser illumination), and indicate a SNR improvement of ~ 23 -fold when using the in-line apparatus. Corresponding

temperature calibration plots obtained using the ‘orthogonal’ and ‘in-line’ set-ups are shown, respectively, in **c** and **d** with R-square values of 0.94 and 0.99. Oxygen peaks appearing in **b** are due to contributions from atmospheric O_2 in the optical path (but outside of the SEOP cell); the contributions from atmospheric N_2 and O_2 were found to be negligible in determining T_{N_2} under present conditions

Boltzmann model and hence, more imprecise temperature measurements compared to results obtained simply by fitting the spectra without subtraction. In any case, when combined with CCD detection (as opposed to using a photomultiplier tube to collect the Raman-scattered photons), the in-line module provides an improvement in SNR compared to the previous orthogonal set-up used by Walter et al. [18], according to calculations considering the acquisition time for a given spectral window of equivalent gas loading and the corresponding spectral SNR obtained.

Once optimised and calibrated, the in-line module was used to demonstrate the in situ measurement of the gas mix temperature inside cells during Rb/ ^{129}Xe spin-exchange optical pumping. For example, we evaluated the effects of pump laser-induced cell heating by comparing the spatial profile (along the x -axis) of T_{N_2} (Fig. 3a) using both frequency-narrowed (Fig. 3c) and broadband (Fig. 3d) laser diode arrays, both operating at 60 W, after only 5 min of optical pumping. N_2 rotational Raman spectra were measured transversely as a function of position across the cell (~ 21 mm behind the front window) at 1 mm intervals, perpendicular to the main pump laser beam (Fig. 3b); these spectra were then converted to temperatures as described above. Illumination by the broadband pump laser resulted in internal gas temperatures (as manifested by T_{N_2} values)

that were ~ 40 °C in excess of T_{cell} , and the temperature (measured via thermocouple) from the forced air oven used to externally heat the OP cell. On the other hand, the dramatically increased resonant energy emitted by the frequency-narrowed laser gave rise to T_{N_2} values that were ~ 200 °C elevated relative to T_{cell} .¹ Figure 3 also showcases the ability of the in-line module to spatially translate to collect data from different regions of the OP cell.

We also used the frequency-narrowed laser to examine the relationship between illuminated laser powers and ΔT_{N_2} ($T_{N_2} - T_{\text{cell}}$) for various external oven cell temperatures, Fig. 4. We found a quasi-linear dependence of ΔT_{N_2} on emitted laser power for each oven temperature setting, with the largest increase in ΔT_{N_2} observed at the highest laser powers and T_{cell} . The fact that the slope of the lines rises with T_{cell} is likely explained by concomitant increases in Rb density [26]; the increased concentration of gaseous absorbers of the incident laser light will drive up the energy deposition rate into the N_2 ro-vibrational degrees of freedom. Moreover, the absorber concentration will also

¹ The much larger differences between internal (gas) and external (wall/oven) temperatures measured in ref [19] likely reflect the much longer optical pumping times for those experiments (allowing more thermal energy to accumulate within the cell), as well as any gas mixture-dependent effects.

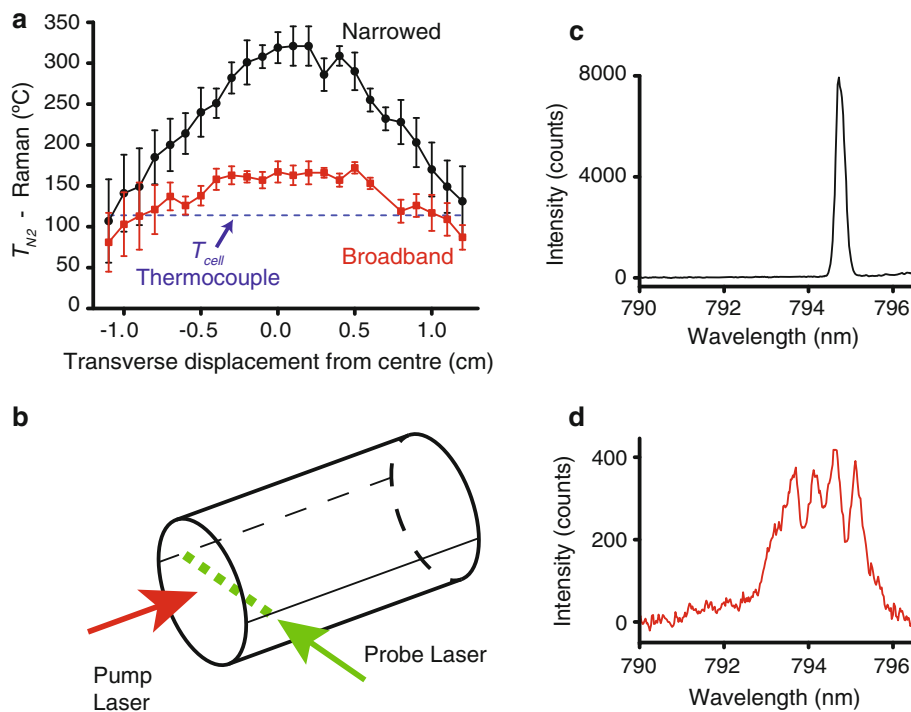


Fig. 3 **a** Plots showing the spatial variation of the steady-state values of T_{N_2} during SEOP, as induced by the ‘pump’ LDAs [acquired after 5 min of illumination by either a 60 W broadband (red squares) or 60 W VHG-narrowed LDA [14] (black circles)]. Plots are compared to the temperature of the external glass wall near the front of the cell, as measured with a thermocouple (dotted line); T_{cell} values were 110 and 150 °C near the front and back of the cell, respectively (lines are

meant to guide the eye). Values for T_{N_2} (three-second integration time) were measured in 1-mm increments by translating the focused spot horizontally across the cross-section of the cell, transverse to the pump beam (**b**). The spectral profiles of the VHG-narrowed and broadband LDAs are shown, respectively, in **c** and **d**; FWHM = 0.26 and 2.13 nm

increase as P_{Rb} suffers from poorer cell illumination [13]; these effects can be rapidly compounded as macroscopic heating from the laser absorption drives more Rb atoms into the vapour phase, increasing the optical density of the cell, which then further increases the laser absorption, thereby fuelling the ‘Rb runaway’ positive feedback loop

[14, 27]. On the other hand, it appears that SEOP performed at lower T_{cell} values gives rise to relatively stable T_{N_2} behaviour, Fig. 4, as many of the available photons are not absorbed, as monitored by the laser power meter behind the cell.

4 Summary

We have implemented a new in-line Raman module for rapidly measuring local internal gas temperatures during SEOP. This apparatus, which obtains N_2 rotational temperatures by probing the ultra-low frequency Stokes/anti-Stokes Raman lines, was shown to provide improvements in detection sensitivity (SNR increase ~ 23 -fold, with corresponding gains in spatiotemporal resolution), accuracy and precision in determining T_{N_2} values, and ease of use compared to our previous orthogonal arrangement. The utility of the in-line approach was demonstrated by exploring the effects of laser heating during SEOP as a function of pump laser power, linewidth, and position within the OP cell. Future experiments will use this in-line module to dynamically probe T_{N_2} for a variety of SEOP parameters, most notably at elevated resonant pump laser powers and as a function of gas mixture, where the benefits

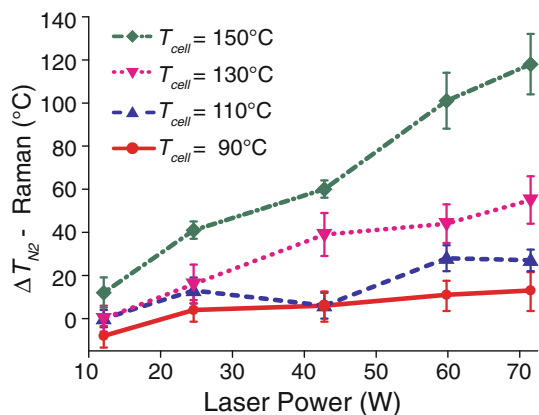


Fig. 4 The temperature difference between T_{N_2} and T_{cell} (ΔT_{N_2}) measured in the middle of the OP cell after 2-min pump laser illumination, plotted as a function of pump laser power for T_{cell} values ranging from 90–150 °C

of greater understanding of energy transport and thermalisation processes during SEOP can be directly translated to improved designs and practices for next-generation clinical polarisers for ^{129}Xe , as well as other noble gas isotopes.

Acknowledgments We thank S. Fitzgerald, W. Twigger, R. Senghani, and A. Knowles (Horiba Jobin–Yvon) for experimental assistance and loan of equipment, as well as Prof. A. Compaan (U. of Toledo) for helpful discussions. H. Newton is funded by an EPSRC studentship. N. Whiting is an NSF International Research Fellow (OISE 0966393). B.M. Goodson is a Cottrell Scholar of Research Corporation. Work at Southern Illinois University Carbondale is supported by DoD CDMRP (W81XWH-12-1-0159/BC112431) and SIUC OSPA. M.J. Barlow acknowledges the School of Clinical Sciences, University of Nottingham and ESPRC grant EP/G003076/1.

References

1. B.M. Goodson, *J. Magn. Reson.* **155**, 157 (2002)
2. I. Dregely, J.P. Mugler III, I.C. Ruset, T.A. Altes, J.F. Mata, W. Miller, J. Ketel, S. Ketel, J. Distelbrink, F.W. Hersman, K. Ruppert, *J. Magn. Reson.* **33**, 1052 (2011)
3. S. Sivaram Kaushik, Z.I. Cleveland, G.P. Cofer, G. Metz, D. Beaver, J. Nouls, M. Kraft, W. Auffermann, J. Wolber, H.P. McAdams, B. Driehuys, *Magn. Reson. Med.* **65**, 1155 (2011)
4. X. Xu, G. Norquay, S.R. Parnell, M.H. Deppe, S. Ajraoui, R. Hashoian, H. Marshall, P.D. Griffiths, J. Parra-Robles, J.M. Wild, *Magn. Reson. Med.* **68**(6), 1900 (2012)
5. A. Nossov, E. Haddad, F. Guenneau, C. Mignon, A. Gedeon, D. Grosso, F. Babonneau, C. Bonhomme, C. Sanchez, *Chem. Commun.* **21**, 2476 (2002)
6. G. Huber, L. Beguin, H. Desvaux, T. Brotin, H.A. Fogarty, J.P. Dutasta, P. Berthault, *J. Phys. Chem. A* **112**(45), 11363 (2008)
7. T. Meldrum, K.L. Seim, V.S. Bajaj, K.K. Palaniappan, W. Wu, M.B. Francis, D.E. Wemmer, A. Pines, *J. Am. Chem. Soc.* **132**(17), 5936 (2010)
8. Y.-Q. Song, B.M. Goodson, R.E. Taylor, D.D. Laws, G. Navon, A. Pines, *Angew. Chem. Int. Ed. Engl.* **36**(21), 2368 (1997)
9. L. Dubois, P. Da Silva, C. Landon, J.G. Huber, M. Ponchet, F. Vovelle, P. Berthault, H. Desvaux, *J. Am. Chem. Soc.* **126**(48), 15738 (2004)
10. R. T. Kouzes, U.S. Department of energy, PNNL-18388 (2009)
11. T.G. Walker, W. Happer, *Rev. Mod. Phys.* **69**(2), 629 (1997)
12. N. Whiting, N.A. Eschmann, B.M. Goodson, M.J. Barlow, *Phys. Rev. A* **83**, 053428 (2011)
13. P. Nikolaou, N. Whiting, N.A. Eschmann, K.E. Chaffee, B.M. Goodson, M.J. Barlow, *J. Magn. Res.* **197**, 249 (2009)
14. N. Whiting, P. Nikolaou, N. Eschmann, M. Barlow, R. Lammer, J. Ungar, W. Hu, L. Vaissie, B. Goodson, *Appl. Phys. B.* **106**, 775 (2012)
15. P. Nikolaou, A. Coffey, L. Walkup, B. Gust, N. Whiting, H. Newton, S. Barcus, I. Muradyan, M. Dabaghyan, G. D. Moroz, M. Rosen, S. Patz, M. J. Barlow, E. Chekmenev, and B. M. Goodson, *Proc. Natl. Acad. Sci. USA* (accepted) (2013)
16. P. Nikolaou, A. Coffey, L. Walkup, B. Gust, H. Newton, I. Muradyan, M. Rosen, S. Patz, M. J. Barlow, B. M. Goodson, and E. Chekmenev, presented at the 54th ENC, Pacific Grove, 2013
17. I. Saha, P. Nikolaou, N. Whiting, B.M. Goodson, *Chem. Phys. Lett.* **428**, 268 (2006)
18. D.K. Walter, W.M. Griffith, W. Happer, *Phys. Rev. Lett.* **86**, 3264 (2001)
19. N. Whiting, H. Newton, M. J. Barlow, P. Morris, and B. M. Goodson (manuscript in preparation) (2013)
20. N. Whiting, H. Newton, M. J. Barlow, P. Morris, and B. M. Goodson, Presented at the 53rd ENC, Miami, (2012)
21. S.R. Parnell, M.H. Deppe, S. Ajraoui, J. Parra-Roubles, S. Boag, J.M. Wild, *J. Appl. Phys.* **107**, 094904 (2010)
22. A. Fink, D. Baumer, E. Brunner, *Phys. Rev. A* **72**, 053411 (2005)
23. R.S. Hickman, L.H. Liang, *Rev. Sci. Instrum.* **43**(5), 796 (1972)
24. C. Moser and F. Havermeier, United States patent 8184285 (2012)
25. G.W. Faris, R.A. Copeland, *Appl. Opt.* **36**(12), 2684 (1997)
26. D. A. Steck, “Rubidium 87 D line data,” available online at <http://steck.us/alkalidata>. Revision 2.1.4. (2010)
27. A.L. Zook, B.B. Adhyaru, C.R. Bowers, *J. Magn. Reson.* **159**(2), 175 (2002)